Permanent earthquake-induced actions in buried pipelines

Permanent Earthquake-Induced Actions in Buried Pipelines: Numerical Modeling and Experimental Verification

G. C. Sarvanis[a], *S. A. Karamanos*[a,b] [1], *P. Vazouras*[a], *E. Mecozzi*[c], *A. Lucci*[c], *P. Dakoulas*[a]

[a] *University of Thessaly, Volos, Greece*

[b] *The University of Edinburgh, Scotland, UK*

[c] *Centro Sviluppo Materiali, Rome, Italy*

ABSTRACT

Buried pipelines are often constructed in seismic and other geohazards areas, where severe ground deformations may induce severe strains in the pipeline. Calculation of those strains is essential for assessing pipeline integrity and, therefore, the development of efficient models accounting for soil-pipe interaction is required. The present paper is aiming at developing efficient tools for calculating ground-induced deformation on buried pipelines, often triggered by earthquake action, in the form of fault rupture, liquefaction-induced lateral spreading, soil subsidence, or landslide. Soil-pipe interaction is investigated using advanced numerical tools, which employ solid elements for the soil, shell elements for the pipe and account for soil-pipe interaction, supported by large-scale experiments. Soil-pipe interaction in axial and transverse directions is evaluated first, using results from special-purpose experiments and finite element simulations. The comparison between experimental and numerical results offers valuable information on key material parameters, necessary for accurate simulation of soil-pipe interaction. Furthermore reference is made to relevant provisions of design recommendations. Using the finite element models, calibrated from these experiments, pipeline performance at seismic-fault crossings is analyzed, emphasizing on soil-pipe interaction effects in the axial direction. The second part refers to full-scale experiments, performed on a unique testing device. These experiments are modeled with the finite element tools, to verify their efficiency in simulating soil-pipe response under landslide or strike-slip fault movement. The large-scale experimental results compare very well with the numerical predictions, verifying the capability of the finite element models for accurate prediction of pipeline response under permanent earthquake-induced ground deformations.

1 INTRODUCTION

The construction of buried pipelines in seismic and other geohazard areas imposes major challenges for their structural integrity. In particular, active seismic faults, liquefaction areas or slope instability regions are associated with large ground deformations that may induce significant strains in the pipeline wall, leading to local buckling and/or rupture and loss of containment. The safer approach against geohazards would be to avoid those dangerous areas, through an appropriate pipeline alignment, but in most cases this may not be a feasible option. As an example, a large number of seismic faults usually exists in high seismicity areas, resulting in numerous fault crossings of the pipeline. In these cases, pipeline design should account for the ground-induced strains due to the differential ground movement at fault location, in addition to the strains developed from operational loads.

The analytical model proposed by Newmark and Hall [1] has been pioneering in predicting ground-induced actions in buried pipelines, focusing on a buried pipeline crossing a seismic fault. Continuing the work in [1], Kennedy *et al.* [2] proposed an enhanced semi-analytical model, considering a non-uniform friction interface between the pipe and the soil. Wang and Yeh [3] further improved this methodology, incorporating pipeline bending stiffness. More recently, Takada *et al.* [4] developed a method for obtaining the maximum strain in buried steel pipelines considering non-linearity of material and geometry of pipe cross-section, while Karamitros *et al.* [5] proposed a semi-analytical elastic-plastic method that requires a numerical solution for calculating the strain induced in the pipeline, in a strike-slip fault crossing. In subsequent publications, Trifonov *et al.* [6,7] and Karamitros *et al.* [8] developed semi-analytical models for analyzing buried pipelines crossing strike-slip (horizontal) and normal faults.

Apart from the above analytical and semi-analytical methodologies, there is an increasing number of reported investigations on the simulation of the buried pipelines under permanent ground actions using numerical finite element models. There exist two types of finite elements models, used for this problem. The first type considers beam-type elements, often referred to as "pipe-elements", for the simulation of pipeline, and non-linear springs for modeling the soil. This type of model has been proposed in several design guidelines and recommendations, such as the ASCE guidelines [9] or the ALA guidelines [10], and has been used extensively for pipeline design purposes. The second type of models employ shell elements for the pipe and solid elements for the surrounding soil; it is more advanced, requiring significant modelling expertise. The rigorous models have been initially introduced by Vazouras *et al.* [11] and also adopted in the recent papers by Trifonov [12] and Kaya *et al.* [13]. As an alternative to the rigorous models, Karamitros *et al.* [5] proposed a "hybrid" numerical approach that employs shell

[1] *Corresponding author*: spyros.karamanos@ed.ac.uk

elements for the pipe and non-linear springs for the soil.

In contrast to the above relatively large number of publications on analytical and numerical methodologies, there exist only a limited number of publications reporting full-scale experimental results on soil-pipe interaction under severe ground actions. Trautmann and O'Rourke [14] were the first to report test data related to transverse force-displacement response of buried pipelines, investigating the effects of pipe diameter, pipe buried depth, pipe roughness and soil density. Ha *et al.* [15] presented results from four centrifuge tests, designed to examine the influence of pipe-fault orientation on pipe behavior under earthquake faulting. Paulin *et al.* [16] and Anderson [17] performed full-scale axial pull-out pipe tests in both "loose" and "dense" sand; they concluded that in dense sand the axial load resistance is substantially higher than the corresponding axial load in the case of loose sand, while the predictions of axial soil resistance offered by ASCE guidelines [9] have been found consistently lower than the experimental results. Scarpelli *et al*. [18] investigated axial soil-pipe interaction performing a series of in-situ tests, together with laboratory interface tests, whereas Mortara *et al*. [19] proposed a two-dimensional constitutive model for investigating solid-soil interaction under cyclic loading. Notable experiments on both transverse and axial response of buried pipelines have also been reported by Karimian [20]; in those tests, the lower prediction for the maximum axial resistance provided by ASCE guidelines [9] with respect to the experimental results for the case of dense sand has been noticed. Moreover, a new methodology has been proposed in [20] for the calculation of maximum axial soil resistance using an equivalent lateral earth pressure coefficient.

Recently, the problem of buried pipelines subjected to permanent ground deformation has been investigated in detail in the framework of European research project GIPIPE [21], using a wide spectrum of numerical, experimental and analytical methodologies. In that project, rigorous numerical simulations of pipeline behavior have been performed and presented in [22-23] and in [24] for strike-slip and normal faults respectively, extending the finite element models introduced in [11], whereas simple and efficient analytical methodologies have also been developed in [25] leading to a straightforward analytical methodology for calculating pipeline strains that employs closed-form expressions. Furthermore, Van Es and Gresnigt [26] developed a unique laboratory set-up to investigate experimentally the behavior of buried steel pipelines under strike-slip faults, using collapsible tubes attached to the pipe to account for soil response in an indirect yet efficiency manner, whereas small-scale tests on normal fault action have been conducted and presented in [24] for the purpose of calibrating their numerical models. In addition to those tests an important contribution of this project has been the performance of large-scale tests to determine soil-pipeline interaction subjected to ground-induced actions. A first brief description and initial evaluation of those large-scale tests has been reported in [27], and are examined in the present paper in detail.

The study presented herein, focusses on the mechanics of soil-pipe interaction under earthquake-induced ground deformations, using the large-scale experiments and the advanced numerical simulation tools developed within the GIPIPE project [21]. More specifically, the present paper has a dual purpose: (a) to identify key material parameters necessary for realistic and efficient prediction of soil-pipe interaction in the axial and the transverse direction of the pipe and (b) to validate advanced numerical tools for pipeline analysis developed by the authors for modeling the effect of severe permanent ground-induced actions on buried pipelines [11, 22, 23]. Following a brief overview of the test program, as well as the presentation of soil properties, the numerical models, employed for the purposes of the present simulations, are described in section 2, with emphasis on soil constitutive modelling. In sections 3 and 4, six tests are described on soil-pipe interaction in the axial direction (three tests) and the horizontal-transverse direction (three tests), followed by detailed numerical simulations for the purpose of calibration of the numerical models. Moreover, using the calibrated numerical models, the effects of axial soil-pipe interaction on the mechanical response of a pipeline crossing a strike-slip fault are also investigated in detail. In section 5, four tests on a unique large-scale "landslide/fault" experimental device are described and simulated rigorously, for the purpose of verifying the efficiency of the finite element models in predicting the mechanical behavior of buried pipelines, subjected to severe ground-induced deformations. Finally, section 6 summarizes some important conclusions from the above experimental and simulation activities.

2 TEST OVERVIEW, SOIL PROPERTIES AND NUMERICAL MODELING

The experimental program described in the present paper consists of a total of ten (10) tests. In the first part of the work, six (6) soil-pipe interaction tests have been performed. More specifically, three (3) tests refer to axial soil-pipe interaction (denoted as "AX"), using a pull-out test configuration, where soil resistance is developed due to friction in the soil-pipe interface, whereas three (3) tests refer to horizontal-transverse soil pipe interaction (denoted as "TR"), representing the dominant soil resistance mechanism in the case of a strike-slip fault or landslide action. The results from those six tests are essential for the purpose of calibrating the numerical finite element models. Furthermore the mechanism of pipe-soil interaction in more complex loading conditions has been investigated by performing four (4) large-scale tests, referred to as "landslide/fault tests" (denoted as "LD"), performed in a special-purpose soil-pipe interaction device. An overview of the experimental testing parameters is presented in Table 1.

In the above experimental program, two different non-cohesive soils have been employed, referred to as "Sand 1" and "Sand 2", and their basic properties are given in Table 2, where ρ is the soil density, φ_{peak} is the maximum value of the internal angle of friction of sand, φ_{res} the residual value of the internal angle of friction while the peak dilation angle of the soil, which is taken equal to $\varphi_{peak} - \varphi_{res}$, is denoted as ψ_{peak}. Moreover the plastic shear strain γ^{p}_{peak} corresponding to φ_{peak}

and the plastic shear strain γ_{res}^{p} corresponding to φ_{res} are also tabulated in Table 2. The soils under consideration have been compacted at water contents between 5.7 % and 8.0 % and their mass density has been measured equal to approximately 1600 kg/m^3. In all tests, the diameter of pipe specimens is equal to 219.6 mm (8 in), the thickness is equal to 5.56 mm and the material is steel grade API 5L X65 (nominal yield stress σ_y equal to 450 MPa). The direct shear tests, from which those data were obtained, were performed by NTUA in the framework of GIPIPE project [21].

Table 1. Overview of experimental testing program.

Test	AX1	AX2	AX3	TR1	TR2	TR3	LD1	LD2	LD3	LD4
Soil	Sand 1	Sand 2	Sand 1	Sand 2	Sand 1	Sand 1	Sand 1	Sand 1	Sand 2	Sand 2
Internal Pressure (MPa)	0	0	0	0	0	0	0	11.4	0	11.4
Coating	Non-coated	Non-coated	Coated	Non-coated	Non-coated	Coated	Non-coated	Non-coated	Non-coated	Non-coated

Table 2. Properties of non-cohesive soil employed in the numerical analysis obtained from direct shear tests.

Soil	Density ρ, (kg/m^3)	Friction angle φ_{peak}	Friction angle φ_{res}	Dilation angle ψ_{peak}	γ_{peak}^{p}	γ_{res}^{p}
Sand 1	1600	45°	37°	8°	0.016	0.09
Sand 2	1600	48.2°	41.7°	6.5°	0.023	0.086

In addition to experimental testing, rigorous finite element models have also been developed to describe numerically the experimental testing procedures. The models employ four-node reduced integration shell elements (type S4R) for modeling the cylindrical pipeline segment, while eight-node reduced-integration "brick" elements (C3D8R) to simulate the surrounding soil. The pipe material is assumed to obey a large-strain von Mises plasticity model, which uses an appropriate stress-strain material curve from uniaxial tension test. The soil constitutive model adopted in the present work follows a modified Mohr-Coulomb approach, also used in previous works by the authors [27]. This is an enhancement of the classical Mohr-Coulomb constitutive model, as described in [28], and has been quite efficient in describing the mechanical behavior of cohesionless soil material, accounting for softening behavior. According to this model, a direct shear test is required to determine the plastic shear strain γ_{peak}^{p} and the plastic shear strain γ_{res}^{p}. The peak dilation angle ψ_{peak} of the soil is taken equal to $\varphi_{peak}-\varphi_{res}$ at plastic shear strain equal to γ_{peak}^{p} and zero for plastic shear strain equal or larger than γ_{res}^{p}. The values of the mobilized dilation angle ψ for intermediate values of plastic shear strain are obtained through a linear interpolation between the γ_{peak}^{p} and γ_{res}^{p} values, which are computed as follows:

$$\gamma_{peak}^{p}=\frac{\delta x_{peak}-\delta x_{y}}{D_{sample}} \tag{1}$$

$$\gamma_{res}^{p}=\gamma_{peak}^{p}+\frac{\delta x_{res}-\delta x_{peak}}{d_{FE}} \tag{2}$$

In equations (1) and (2) the values of δx_{peak} and δx_{res} are the horizontal displacements of the soil sample corresponding to φ_{peak} and φ_{res}, δx_{y} is the horizontal displacement of the soil sample on the onset of yielding, D_{sample} is the initial depth of the soil sample, d_{FE} is the height of the soil elements around the pipe. To define the above material parameters, direct shear tests have been performed in samples of the two sands used in the tests, and the values of φ_{peak}, φ_{res} and ψ_{peak} are given in Table 2. The corresponding values of δx_{peak} and δx_{res} have been measured equal to 1.2 mm and 3.5 mm for Sand 1, and 1.4 mm and 3.3 mm for Sand 2. The results of the direct shear test of Sand 1 are presented in Figure 1.

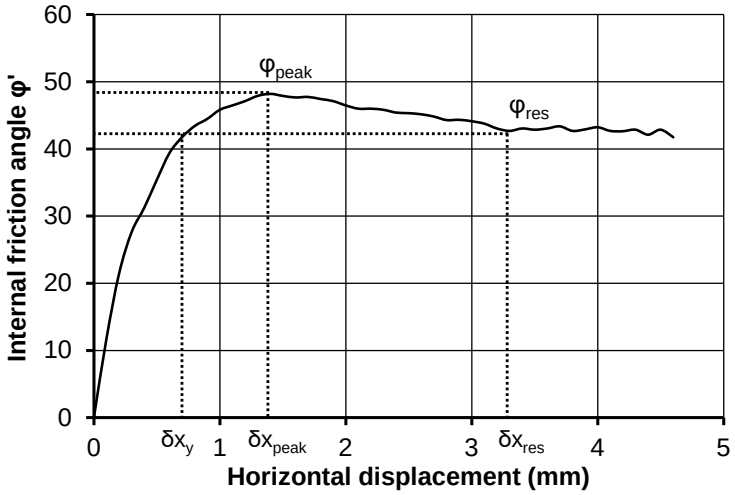

Figure 1. Direct shear test results of Sand 1.

3 AXIAL SOIL-PIPE INTERACTION

3.1 Experimental procedure and results

Soil-pipe interaction in the axial direction of the pipe is discussed in this paragraph, in terms of its effects on the pull-out response of a buried pipe, and the key soil material parameters, necessary for realistic simulation, are identified. In previous pull-out tests (axial) on buried pipelines, reported by Paulin *et al.* [16], Anderson [17] and Karimian [20], it has been noticed that the maximum axial resistance is higher than the resistance predicted by the provisions of the ASCE guidelines [9]. This observation has been noted in all the above tests, and this is an important aspect to be examined in the present study. The experiments have been performed in the test device shown in Figure 2 and Figure 3 referred to as "Full-Scale Test Machine (FSTM)". The FSTM, originally designed to perform mechanical testing on tubular components, was modified by installing a steel box within the testing frame to contain the soil and the pipe. A special-purpose hinge clamping system has been designed to connect the machine frame with the hydraulic actuator, as also shown in Figure 2. The test instrumentation includes a load cell to measure the actuator force, while the stroke is measured by the displacement sensor of the hydraulic actuator. In the present test, only the axial load actuator is used. The pipe surface in contact with the soil is not instrumented, in order to avoid any interference with the soil-pipe interface conditions. The pipe is pulled in the longitudinal axis direction at very low constant speed through special low-friction openings in the soil box that prevent any vertical displacement of the pipe. The applied maximum pipe displacement is such that the pipe far end does not enter into the soil box.

The experimental results from the axial pull-out tests are shown in Figure 4, in terms of the axial pull-out force and the corresponding pull-out (sliding) displacement. Furthermore, the difference between the experimental data and the predictions obtained from ASCE guidelines [9] for test AX1 is shown in Figure 5.

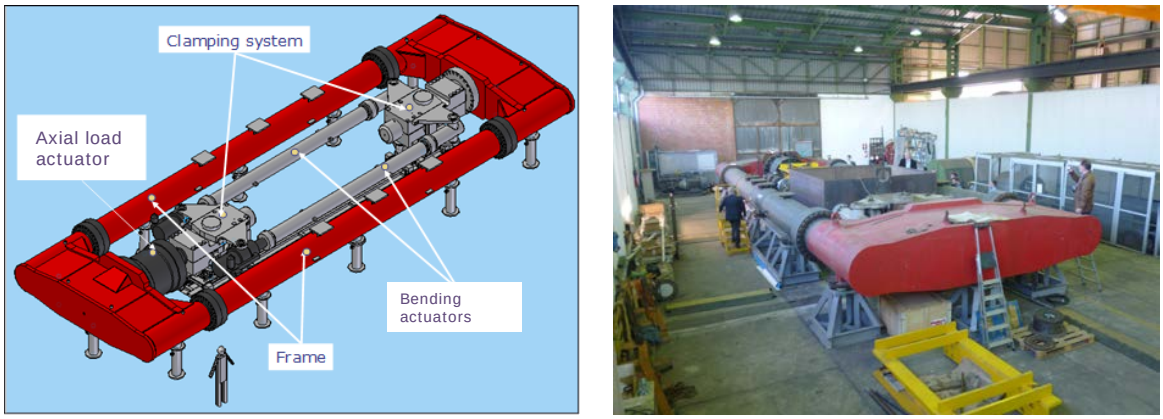

Figure 2. Test device of axial (pull-out) and transverse pipe-soil interaction experiments, CSM facilities, Italy.

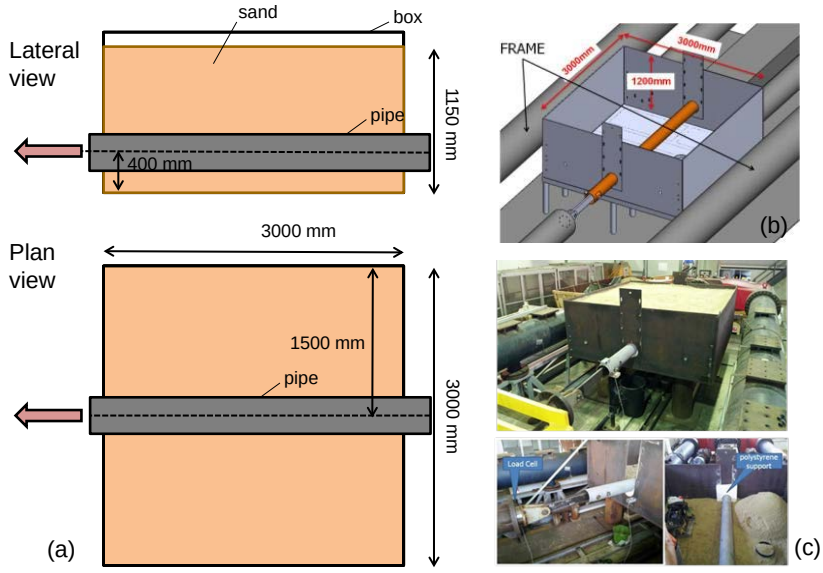

Figure 3. Axial (pull-out) test configuration.

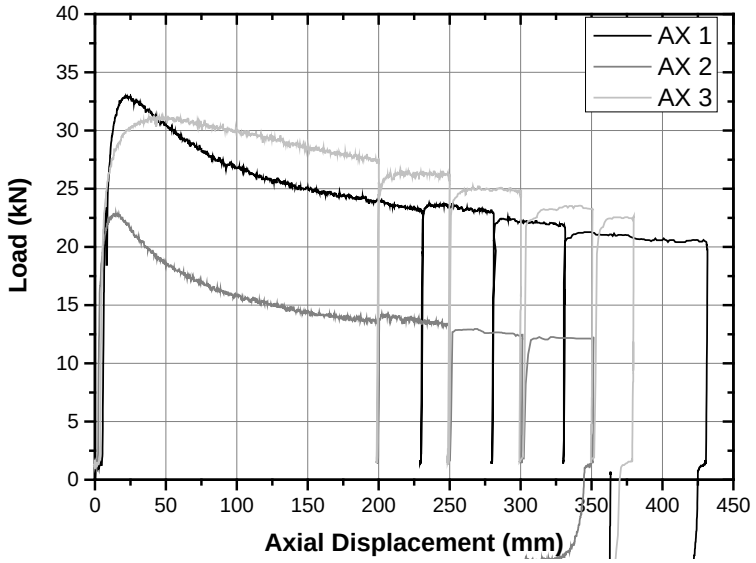

Figure 4. Diagram of pull-out force versus displacement for the three axial tests (AX 1: Sand 1 and non-coated; AX 2: Sand 2 and non-coated; AX 3: Sand 1 and coated).

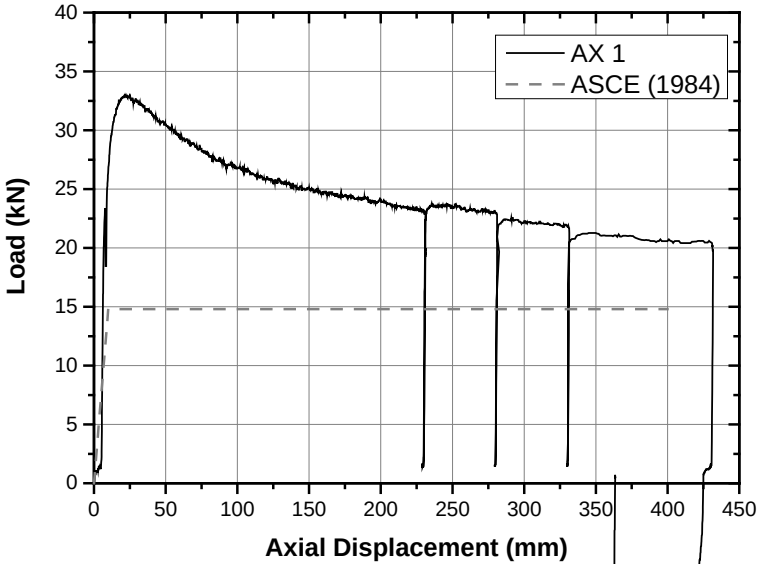

Figure 5. Comparison of experimental results for test AX1 (Sand 1 and non-coated) and the predictions of ASCE guidelines [9].

3.2 Numerical simulation of axial soil-pipe interaction tests

Simulations of the above axial experiments are reported in the present section, in an effort to elucidate soil pipe interaction behavior, extending some previous discussions reported in [27]. In this analysis, an accurate simulation of axial soil-pipe interaction for the soil consideration is crucial. In the case of sand, the maximum soil resistance t_u against pipe movement in the axial pipeline direction, can be expressed by the following equation, adopted by the ASCE guidelines [9]:

$$t_u = \pi D\left(\frac{\sigma_v + \sigma_h}{2}\right)\tan(\delta\varphi) \tag{3}$$

The above equation denotes force per unit pipe length and describes a classical Coulomb friction law, where φ is the internal friction angle, σ_h and σ_v are the lateral and the vertical pressure at the pipe burial depth respectively, and δ is a coefficient, which accounts for reduced friction at the steel-sand interface compared with the friction within the sand. However, Eq. 3, cannot predict satisfactorily soil-pipe interaction in this direction because it does not account for the stress increment $\Delta\sigma$ developed at the soil-pipe interface, due to confined shear conditions in a sand soil with dilatancy; under those conditions the soil may not expand freely and, therefore, an extra stress $\Delta\sigma$ develops in the direction normal to the soil-pipe interface. Figure 6a shows a schematic representation of the shear zone and the additional stress $\Delta\sigma$ developed around the buried pipe, caused by the relative movement between the soil and the pipe. To account for this effect, an enhanced version of Eq. 3 is proposed as follows:

$$t_u(d) = \begin{cases} \dfrac{\pi D d}{d_{crit}}\left[\dfrac{\sigma_v + \sigma_h}{2} + \Delta\sigma_{peak}\right]\tan\delta\varphi_{peak}, & \text{if} \quad d \le d_{crit} \\ \pi D\left[\dfrac{\sigma_v + \sigma_h}{2} + \Delta\sigma(d')\right]\mu(d'), & \text{if} \quad d > d_{crit} \end{cases} \tag{4}$$

where d is the relative axial soil-pipe movement, d_{crit} is the value of d at maximum soil resistance, and functions $\Delta\sigma(d')$ and $\mu(d')$ are given below:

$$\Delta\sigma(d') = \Delta\sigma_{res} + (\Delta\sigma_{peak} - \Delta\sigma_{res})e^{-\alpha d'} \tag{5}$$

$$\mu(d') = \tan\delta\varphi_{res} + (\tan\delta\varphi_{peak} - \tan\delta\varphi_{res})e^{-\alpha d'} \tag{6}$$

In equations (5) and (6), d' is equal to $d - d_{crit}$, while the value of d_{crit} can be taken equal to 2.5 – 5 mm (0.1 – 0.2 in) for dense-to-loose sand, as suggested in [9]. Furthermore, the value of parameter α in Eqs. (5) and (6) controls the rate of soil resistance decay with respect to the relative displacement d and depends on the interface friction and soil volumetric changes during shear. Based on the results of pull-out tests, for δ equal to 0.7 the value of α for the soil under consideration is equal to 9 mm^{-1}. The peak and residual values of the additional stress $\Delta\sigma$, denoted as $\Delta\sigma_{peak}$ and $\Delta\sigma_{res}$ respectively, can be readily computed by performing an one-element test analysis, at which vertical movement of the soil element is restrained, as shown schematically in Figure 6b. The values of $\Delta\sigma_{peak}$ and $\Delta\sigma_{res}$ have been calculated equal to 12.5 kPa and 8.12 kPa for test AX1, and 4.5 kPa and 0 kPa for test AX2, respectively.

Eq. 4 has been implemented in the numerical model for soil-pipe interaction in the axial direction, shown in Figure 7. The finite element model follows the general description reported in section 2, employing shell elements for the steel pipe and solid elements for the soil. To account for axial soil-pipe interaction, a contact algorithm following the decay law of Eq. 4 has been developed and implemented in program ABAQUS [29] in order to describe friction at the soil-pipe interface.

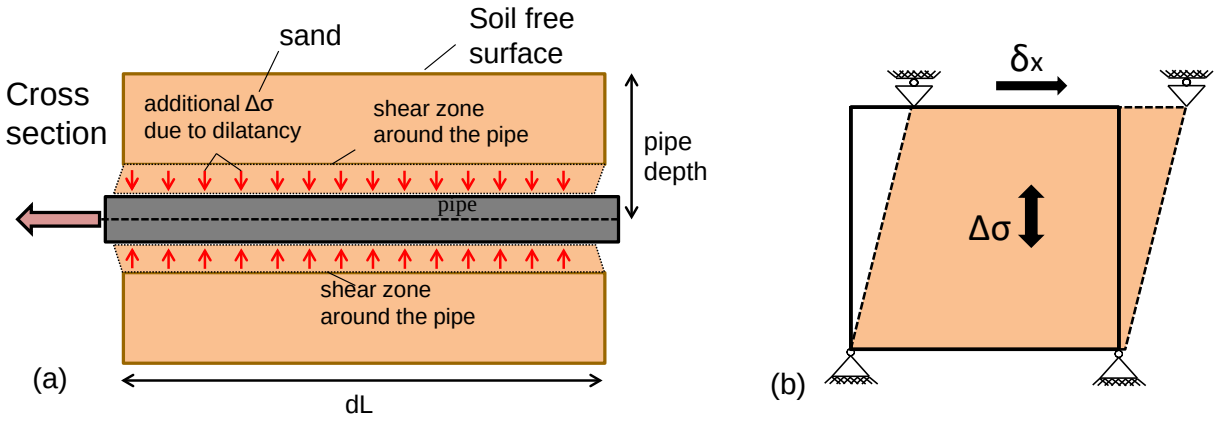

Figure 6. (a) Shear zone around the buried pipe caused by axial relative movement between soil and pipe; (b) one-element numerical model with restrained vertical motion, used for computing the extra stress $\Delta\sigma$ due to dilatancy of the sand soil.

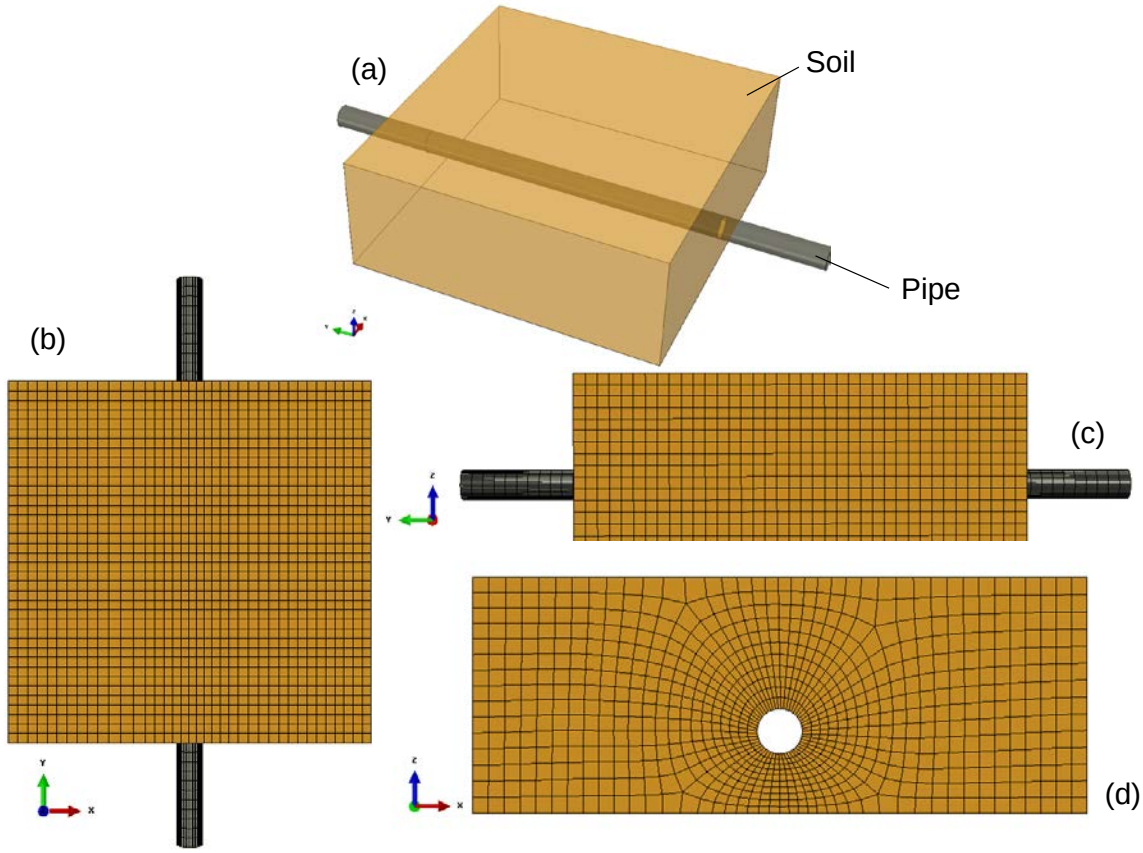

Figure 7. Finite element model for the numerical simulation of the pull-out (axial) tests; (a) 3D view, (b) top view, (c) side view, (d) front view.

Comparisons between the experimental results and numerical calculations using the finite element model of Figure 7 are shown in Figure 8 and Figure 9 for tests AX1 and AX2, respectively. The prediction of soil-pipe interaction, obtained from the finite element analysis, is very satisfactory and representative of the physical problem. The soil conditions of test AX3 are similar to those of test AX1, except for pipe coating. Figure 4 shows that the decay of axial force in test AX3 is different than the one in test AX1, but the peak and residual values are quite similar. Using the finite element model with the decay law of friction corresponding to test AX1, the peak and the residual values can be predicted for test AX3 with fairly good accuracy despite the differences in the decay rate. The effect of friction decay after the peak soil resistance on pipe overall structural performance is investigated in the next paragraph, for the case of a strike-slip crossing configuration.

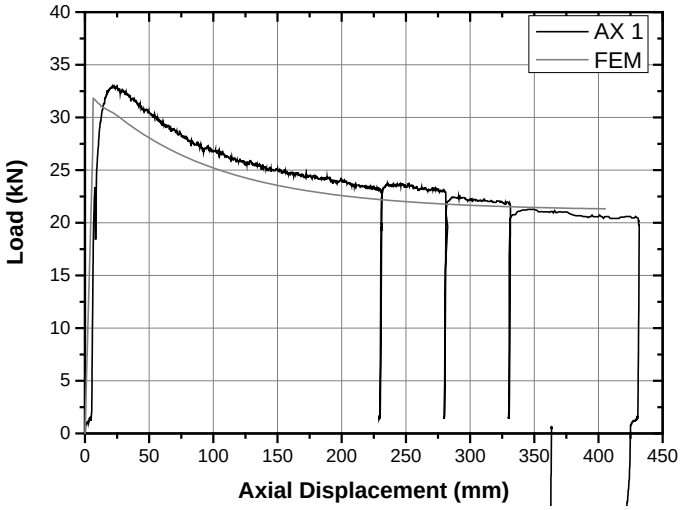

Figure 8. Comparison of experimental results from test AX1 (Sand 1 and non-coated) and finite element predictions.

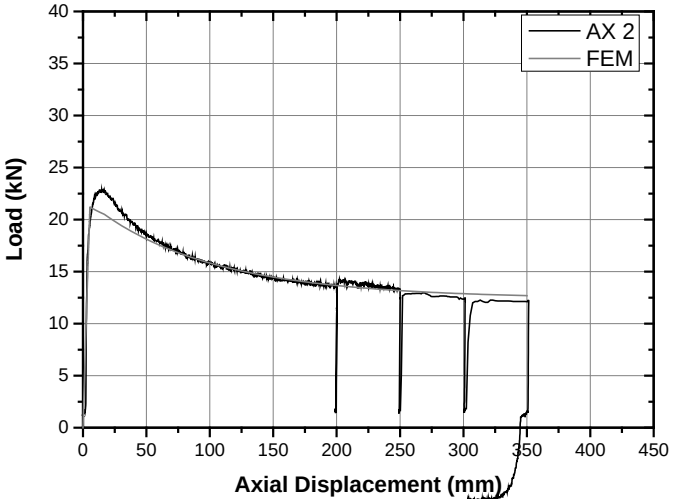

Figure 9. Comparison of experimental results from test AX2 (Sand 2 and non-coated) and finite element predictions.

3.3 Influence of axial soil-pipe interaction on seismic fault-crossing pipeline response

Using the above models for friction at soil-pipe interface, the effects of axial soil resistance on the structural performance are investigated for a pipe crossing strike-slip seismic faults. The numerical study refers to two fault crossing scenarios of a 36-inch diameter (914.4 mm) pipeline with crossing angles β (Figure 10) equal to 0º and 30º. For the pipeline under consideration, two values of thickness t are considered ($\frac{3}{8}$-in and $\frac{1}{2}$-in) and the pipe material is steel grade X65. The burial depth is chosen equal to 2 meters below the ground surface, which is represented by the top surface in Figure 10. According to [11] a 60-meter-long segment of the pipeline is considered, and modelled with shell elements, whereas the soil prism dimensions in directions x, y and z are equal to 60, 10 and 5 meters, respectively. Those dimensions are adequate for the purposes of the present study. The dimensions of the model are also shown in Figure 12. The analysis is conducted in two steps: gravity loading is applied first and, subsequently, fault movement is imposed. The soil parameters are those of Sand 1 used in the experimental testing. Four different cases of axial pipe soil interaction have been examined in this parametric analysis, and the force-displacement curves of each "pipe-soil interaction" are shown in Figure 11. The first case, referred to as "*ASCE*", corresponds to the soil resistance proposed by ASCE guidelines [9], whereas the second case, referred to as "*peak*", assumes a bilinear friction law corresponding to the peak value of the actual behavior. The third case, referred to as "*residual*", assumes a bilinear friction law corresponding to the residual value of the actual behavior, and finally the last case, referred to as "*decay law*", and adopts the actual soil-pipe interaction, as obtained from the axial (pull-out) experiments and modelled with the friction user subroutine presented above.

It is worth noticing that despite the fact that maximum strains due to bending occur with a zone of few meters from the fault, axial soil-pipe interaction is activated in a very long distance along the pipeline, which may be equal to a few hundred meters on either side of the fault area. In order to account for this slow decay of axial deformation a "hybrid" model is adopted, shown in Figure 10. In this model, the area in the vicinity of the seismic fault is simulated with shell elements for the pipe and solid elements for the soil, as shown in the soil block of Figure 12; in that block, significant axial strains/stresses are developed

in the pipe, whereas outside this block the pipeline is simulated with "pipe" elements and the soil with non-linear springs. Appropriate kinematic conditions have been imposed to connect the shell and beam elements at the end of the central 60-meter-long pipe segment.

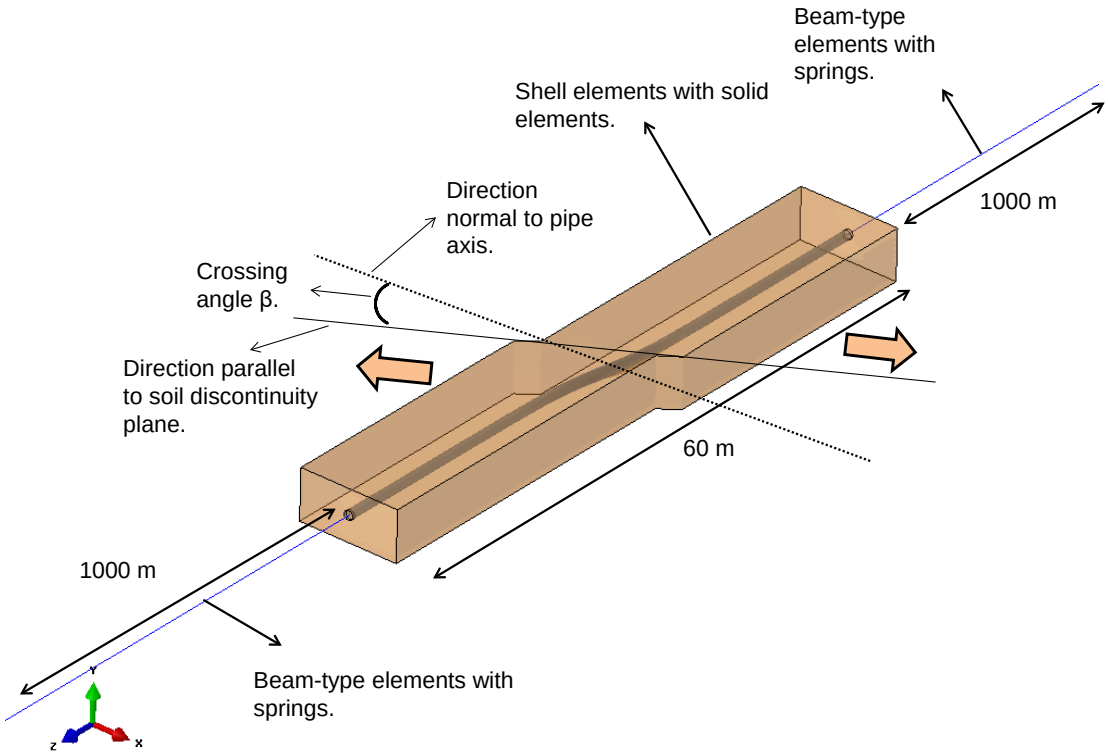

Figure 10. Pipeline configuration in a horizontal (strike-slip) seismic fault crossing; crossing angle β is measured with respect to the direction normal to the pipeline axis.

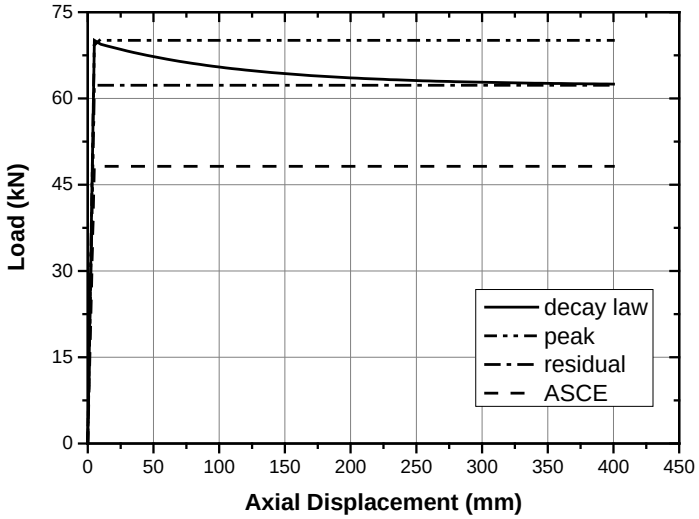

Figure 11. Axial soil-pipe interaction with four different friction conditions, used in the parametric study of seismic fault crossing.

The numerical results for crossing angle β equal to zero (i.e. fault perpendicular to the pipe axis) indicate that the axial soil-pipe interaction has a rather small effect on the structural performance of the pipe for this particular case. Pipe failure occurs approximately at the same ground displacement in all four different cases of axial soil-pipe resistance, for both thicknesses. The results are presented in Figure 13. On the other hand, the numerical results for the case of crossing angle β equal to 30^o indicate that axial soil-pipe resistance may have a significant effect on the structural performance of the pipe for large values of the crossing angle β. The results are presented in Figure 14, in terms of fault displacement corresponding to

tensile strain of the pipe wall equal to 2% and 3%, which may both be considered as reasonable values for tensile strain limit [21]. The fault displacement values corresponding to cases "*decay law*", "*peak*" and "*residual*" are quite similar for both pipe thicknesses analyzed. The results obtained in this parametric analysis indicate that accurate description of the decay law for soil-pipe interaction in the axial direction may not be absolutely necessary. This means that one may use a bilinear friction law (without hardening or softening), corresponding to the peak or the residual value of axial pipe-soil interaction, and obtain reliable results for pipeline performance.

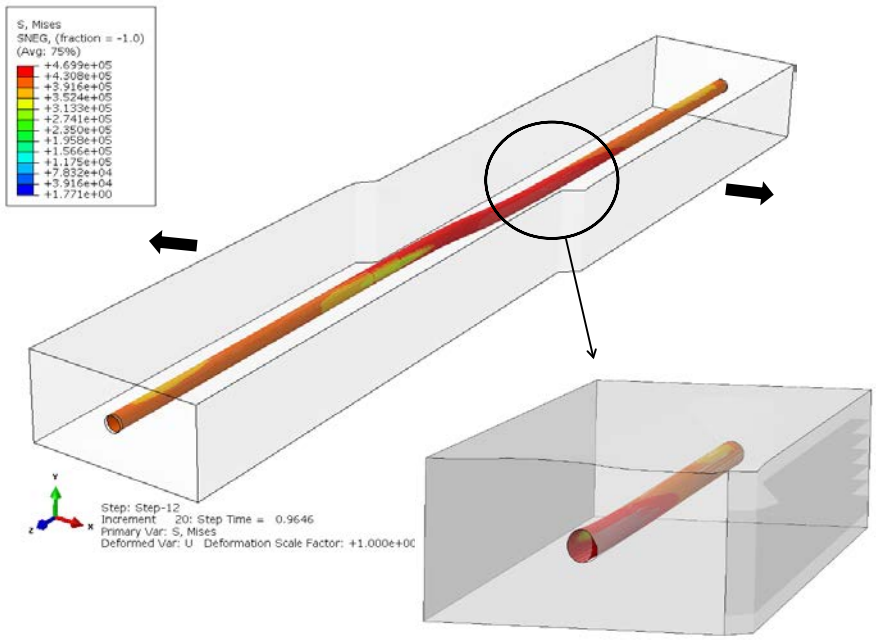

Figure 12. Finite element model for the simulation of pipeline crossing.

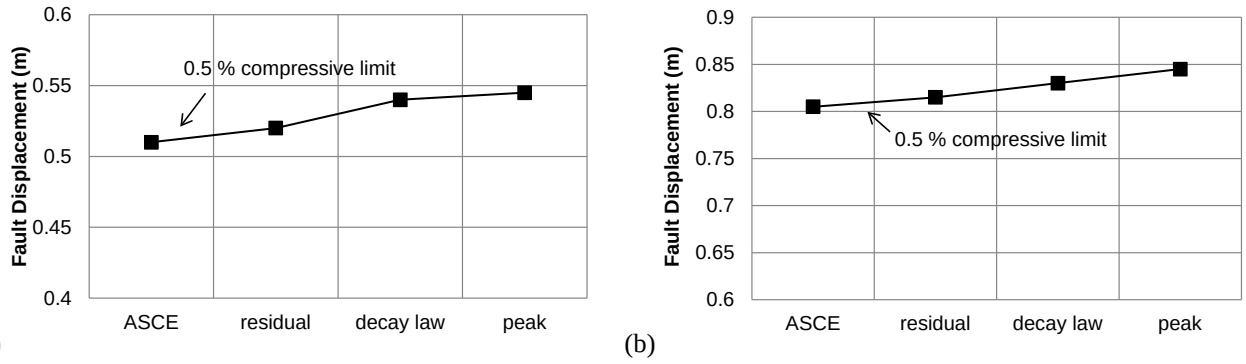

Figure 13. Fault displacement corresponding to 0.5% compressive strain for a 36-inch-diameter, X65 steel pipe with thickness equal to $\frac{3}{8}$ -inch (a) and $\frac{1}{2}$ -inch (b).

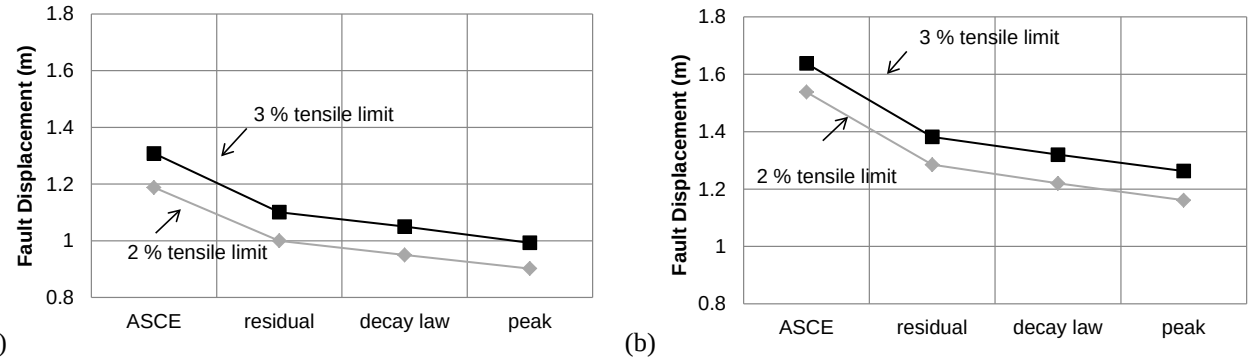

Figure 14. Fault displacement corresponding to 2% and 3% tensile strain for a 36-inch-diameter, X65 steel pipe with thickness equal to $\frac{3}{8}$ -inch (a) and $\frac{1}{2}$ -inch (b).

4 TRANSVERSE SOIL-PIPE INTERACTION

4.1 Experiments on transverse soil-pipe interaction

Soil-pipe interaction in the transverse horizontal direction of a buried pipeline subjected to permanent ground actions plays a significant role in pipe deformation. Three transverse soil-pipe tests have been performed in the course of the present research program, using the experimental setup shown schematically in Figure 15, where the pipe is contained within a steel box and buried in sand. The pipe is pulled horizonally in the transverse direction with respect to its axis at very slow constant speed by means of two pulling bars that penetrate the box wall through small openings. These bars are connected to a stiff beam, bolted to the hydraulic actuator system. The vertical displacement of the pipe is prevented by two parallel horizontal guide rails at the two ends of the pipe specimen (Figure 15b), which also support the self weight of the pipe. To prevent any bending or buckling of the pipe as a result of the two horizontal forces exerted at the two ends, the pipe has been filled with concrete so that the response refers purely to the transverse soil-pipe interaction; furthermore, because of pipe rigidity, contract pressure is assumed uniformly distributed along the length of the specimen. Figure 16 shows the test assembly before backfilling and the deformed shape of the free soil surface after testing.

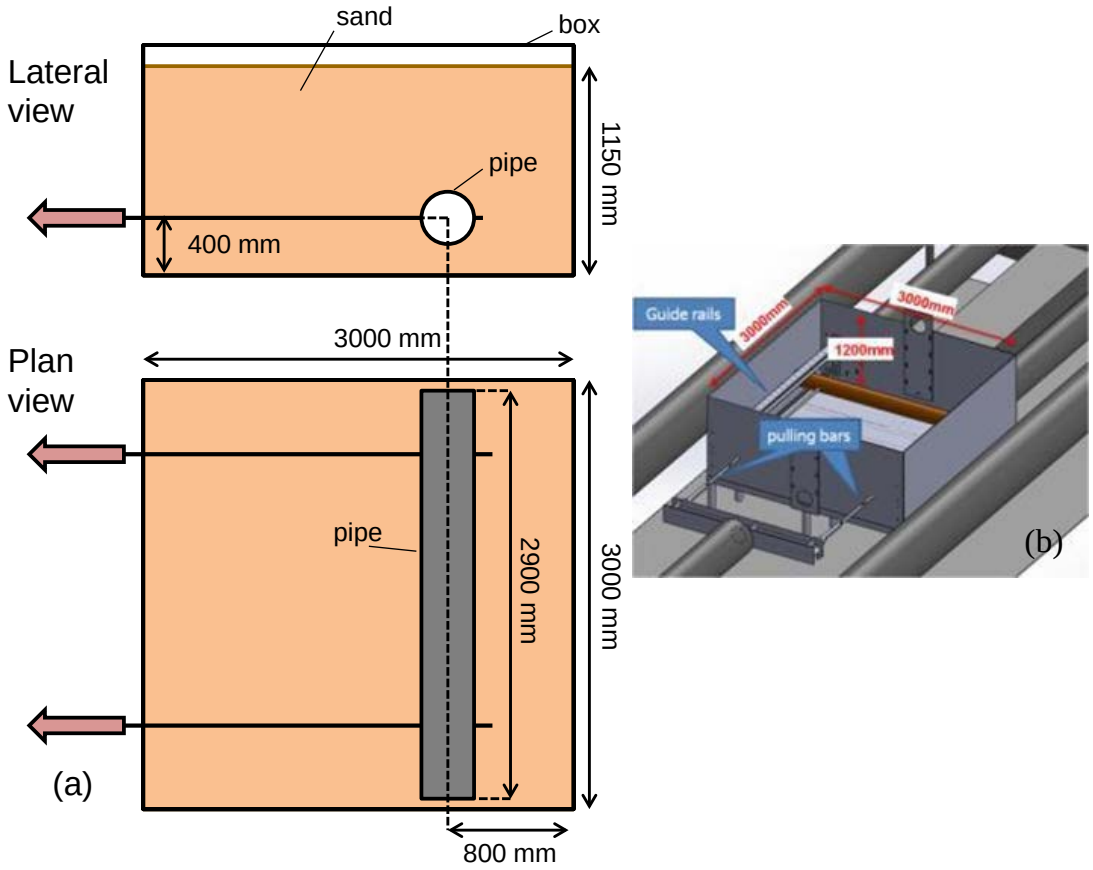

Figure 15. Experimental set-up for transverse pipe-soil interaction; (a) plan view; (b) steel soil box with pipe specimen.

(a)  (b) 

Figure 16. Transverse soil-pipe interaction; (a) test setup before backfilling; (b) soil surface after the test.

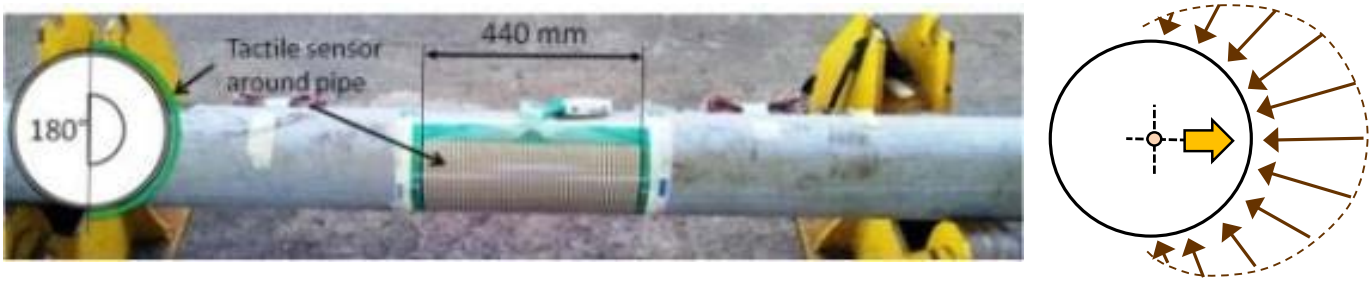

Figure 17. Pressure sensor wrapped around the pipe (left) for measuring soil pressure distribution during pipe motion (right).

The test instrumentation includes a load cell to measure the pulling force, while the stroke is measured by the displacement sensor of the hydraulic actuator. The pipe surface is also instrumented with a flexible contact pressure sensor, as shown in Figure 17, wrapped around a sector of about 180° at the "pulling" (front) side of the pipe and at a width of 440mm along the pipe. The sensor consists of a matrix of 52 × 44 sensing elements. The resulting force exerted by the soil on the pipe can be assumed to be a combination of a distributed load component acting in the direction normal to the pipe surface, and a tangential component resulting from soil friction around the pipe. Therefore, the stresses acting on the pipe surface as a result of soil-pipe interaction (Figure 18a), consists of two components: normal stresses (Figure 18b) and tangential stresses (Figure 18c). In the present case, only the normal stresses are measured by the contact pressure sensor, while the tangential stresses can be estimated from the friction between the pipe and the soil from the following relationship:

$$\tau = \tan(\delta\phi_{res})\, p \tag{7}$$

where p is the pressure acting in the direction normal to pipe surface, δ is a soil-pipe interface coefficient and φ_{res} is soil residual internal friction angle. Referring to Figure 18, the resultant force R acting on the pipe along the displacement direction can be computed with the following relationship:

$$R = R_H + T_H = \sum_{i=1}^{n} p_{mi} A_i \cos\theta_i + \sum_{i=1}^{n} (\tan\delta)\, p_{mi} A_i \sin\theta_i \tag{8}$$

where i denotes the i^{th} row of sensor elements around the circumference located at an angle θ_i, p_{mi} is the average pressure of the i sensor, A_i is the total area of the i^{th} row of sensor element around the circumference.

The results of the three transverse tests are shown in Figure 19 in terms of their load-displacement diagrams, where the reported force refers to the entire 3-meter-long specimen. In Figure 19, the force measured from the load cells and the force calculated from the contact pressure sensors are reported. In all three experiments, the load cell forces are significantly higher than the corresponding pressure sensor forces. This difference is attributed to the extra friction due to compacted sand trapped into the two horizontal guide rails (Figure 15b and Figure 16a). Because of this extra friction, the load cell measurements may not be representative of transverse soil-pipe interaction, and therefore, the force values from the pressure sensor measurements should be employed. The experimental measurements from all three tests indicate a similar load-displacement response, especially for displacement values larger than 400 mm (i.e. larger than 2 pipe diameters).

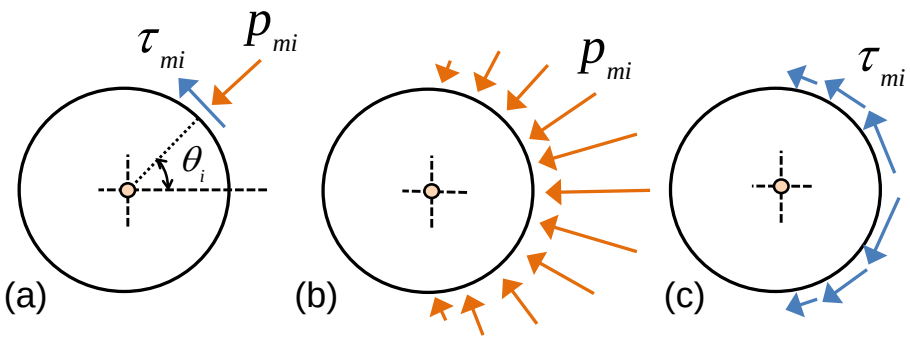

Figure 18. Schematic representation of stresses acting on pipe surface due to soil-pipe interaction in the transverse test: (a) normal and tangential stress components acting on the i^{th} row of the sensor element, (b) normal stresses, (c) tangential stresses due to friction.

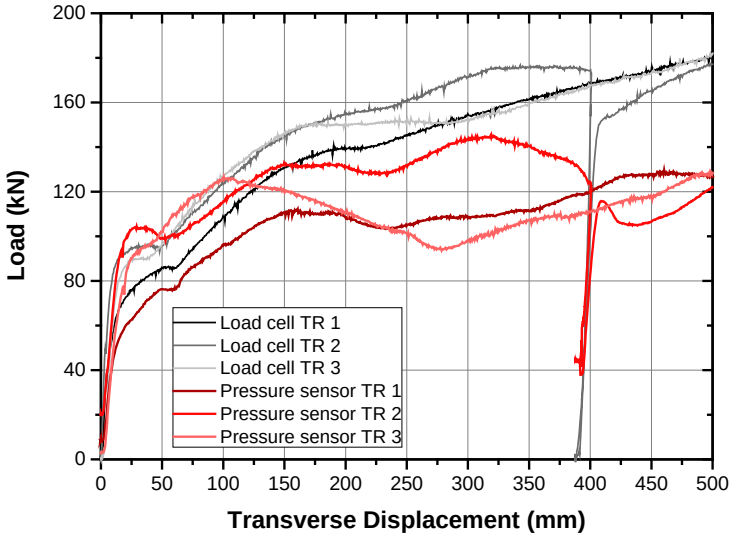

Figure 19. Load-displacement diagrams from the three transverse tests; TR 1 is with Sand 2 and non-coated pipe; TR 2 is with Sand 1 and non-coated pipe; TR 3 is with Sand 1 and coated pipe.

4.2 Finite element simulation of transverse tests

A finite element model has been developed, which follows the general trends described in sections 2 and 3, employing shell elements for the pipe and solid elements for the soil, to simulate the transverse pipe-soil interaction tests. The model, shown in Figure 20, uses the modified Mohr-Coulomb model [28] to model soil behavior. To reduce the computational effort without loss of accuracy, only a slice of the soil/pipe system of width equal to 1m is modeled. In the two vertical faces of the model, correspond to *xy* plane of Figure 20, *z* symmetry has been imposed. The analysis proceeds with a displacement-controlled scheme, moving the pipe in the horizontal transverse direction, as shown in Figure 15, while pipe displacement in the vertical direction is restricted, representing exactly the experimental procedure.

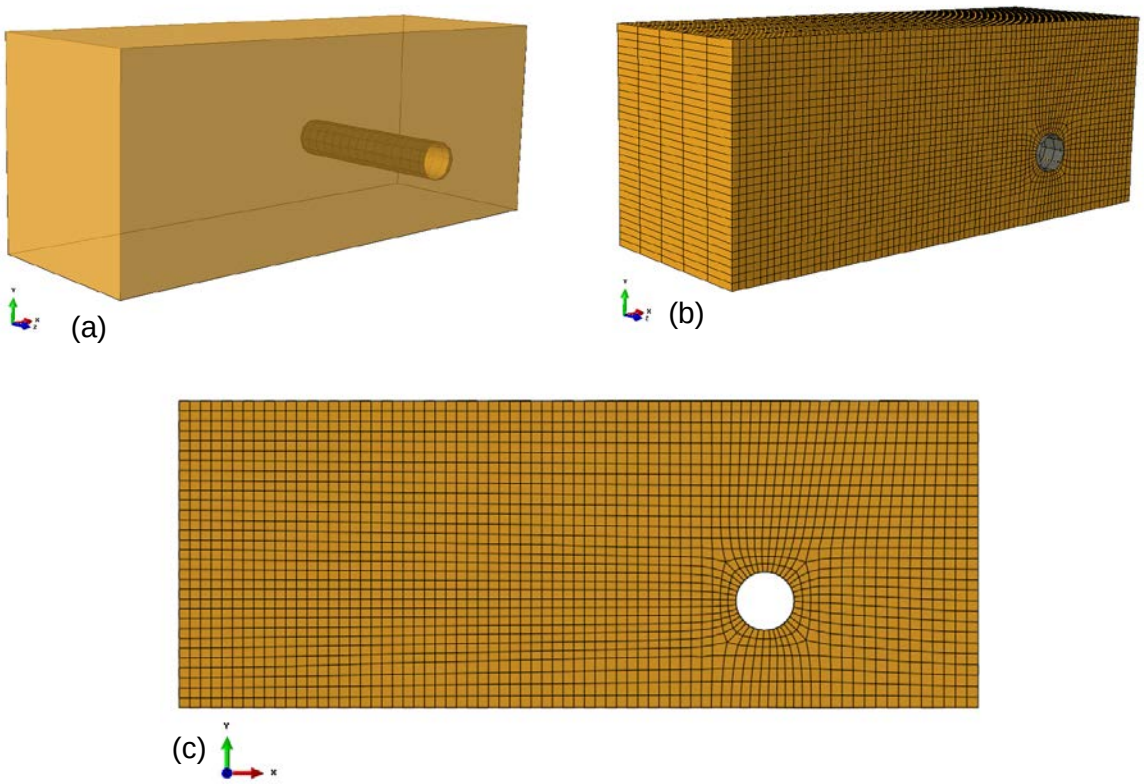

Figure 20. Finite element models for transverse soil-pipe interaction test: (a) three-dimensional view (b) and (c) section view with the finite-element mesh.

The deformed shape of soil block and the distribution of the equivalent plastic strain from the finite element simulation of the transverse test are shown in Figure 21. Comparisons of the load-displacement diagrams obtained experimentally and numerically are shown in Figure 22, Figure 23 and Figure 24 for the three transverse tests TR1, TR2 and TR3, respectively. The comparison shows that the finite element predictions are quite close to the experimental results. Despite the fact that the numerical model may not be very suitable for describing all physical phenomena associated with large deformations of a granular material, this model is shown to be capable of representing accurately soil resistance against pipe movement and simulate efficiently soil-pipe interaction in the transverse direction of the pipe in very good agreement with the test results. Therefore, for purposes of the present study the present model is considered adequate, for simulating transverse soil-pipe interaction and its effects on pipe structural response.

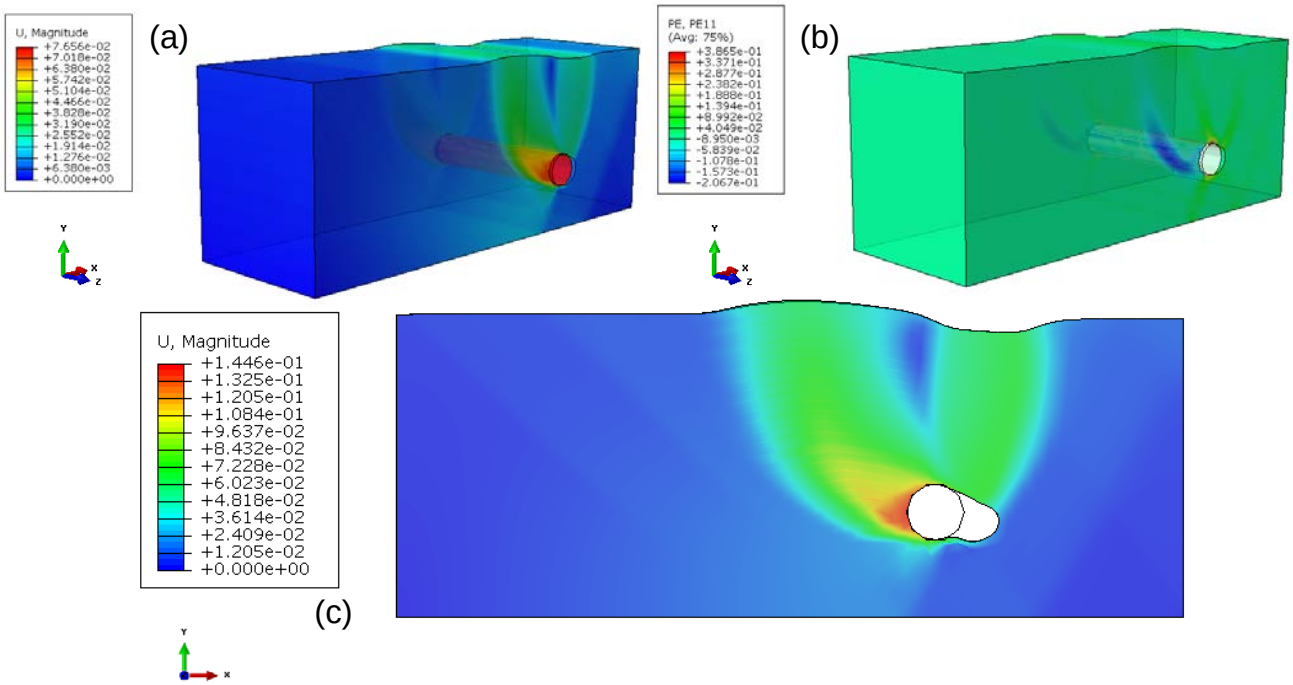

Figure 21. Deformed shape of soil block from finite element simulation of the transverse test: (a) three-dimensional view of displacement field, (b) three-dimensional view of normal plastic strain at horizontal/transverse direction x, (c) two-dimensional view of displacement field.

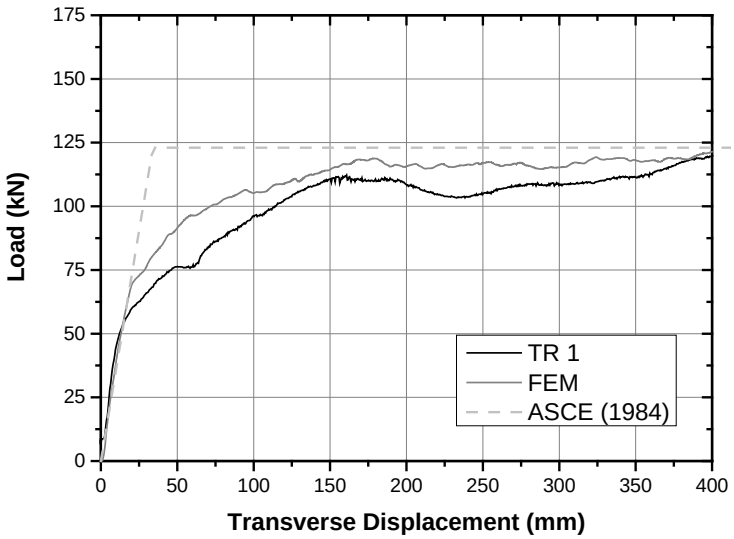

Figure 22. Comparison between the results of transverse test TR1 (Sand 2 and non-coated pipe) and finite element predictions.

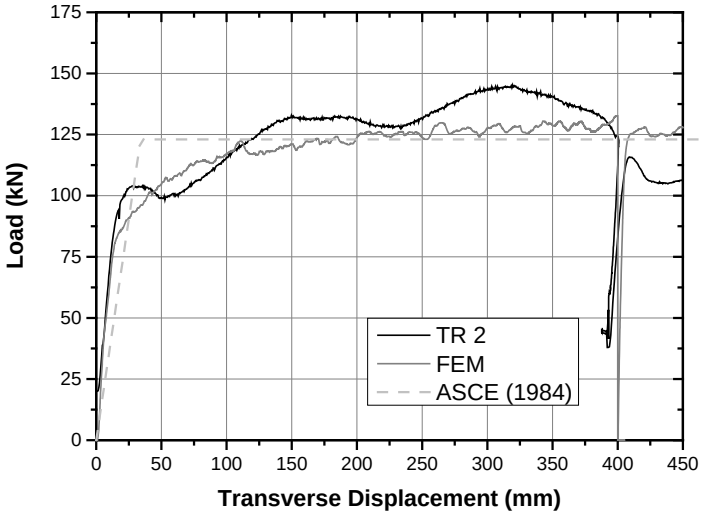

Figure 23. Comparison between the results of transverse test TR2 (Sand 1 and non-coated pipe) and finite element predictions.

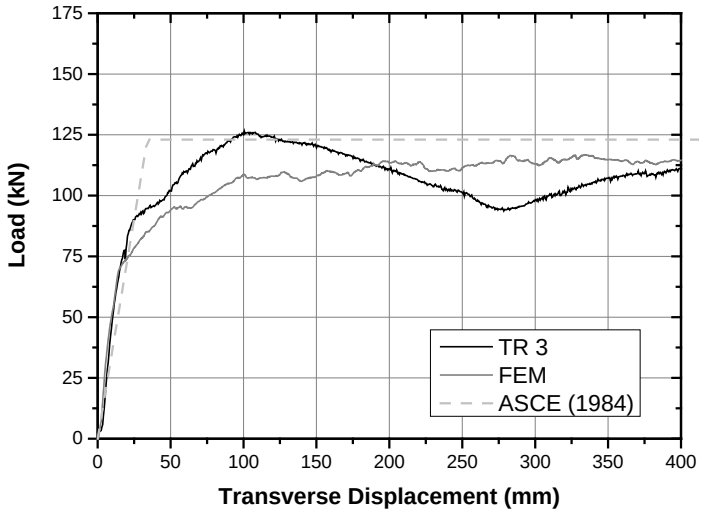

Figure 24. Comparison between the results of transverse test TR3 (Sand 1 and coated pipe) and finite element predictions.

A numerical study has also been performed in order to identify the key soil material parameters for the accurate simulation of this problem, using the test data from experiment TR3. More specifically, three different cases are analyzed, using different soil parameters. In the case referred to as "*residual"*, the sand is simulated with a classical Mohr-Coulomb model with internal friction angle equal to φ_{res} and dilation angle equal to zero. In the case referred to as "*peak"* the classical Mohr-Coulomb model is employed with internal friction equal to φ_{peak} and dilation angle equal to $\psi_{peak} = \varphi_{peak} - \varphi_{res}$. Finally, the case referred to as "*decay law*" employs the modified Mohr-Coulomb model described in the previous paragraphs. The results of this numerical study are shown in Figure 25 in the form of force versus displacement diagram. The "*peak"* case appears to overestimate soil resistance, while the "*residual"* and the "*decay law*" cases provide similar results, indicating that the residual value of internal friction φ_{res} is a dominant parameter for the transversal soil-pipe interaction response. Therefore, one may simulate transverse soil-pipe interaction quite satisfactory by simply using the classical Mohr-Coulomb model with internal friction equal to φ_{res} and dilation angle equal to zero.

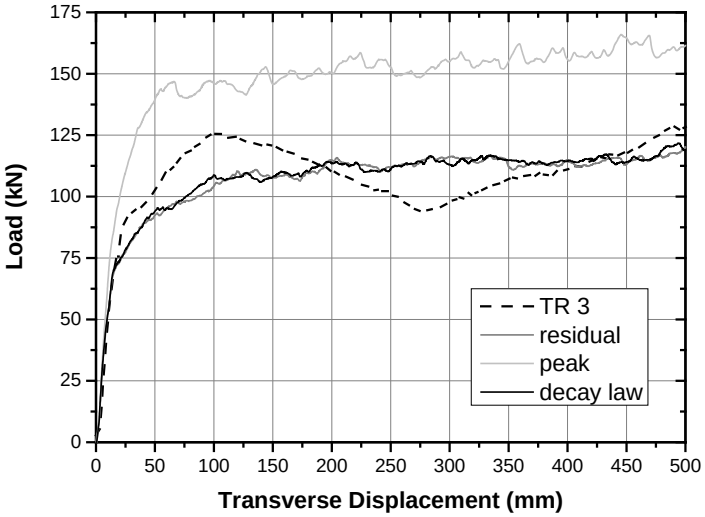

Figure 25. Comparison between the results of transverse soil-pipe interaction test TR3 (Sand 1 and coated pipe) and the three cases considered in the parametric study.

5 LARGE-SCALE LANDSLIDE/FAULT TESTING AND NUMERICAL SIMULATION

5.1 Description of full-scale tests

Large-scale tests have been performed using a special-purpose "landslide/fault" device, in order to investigate pipe-soil interaction in horizontal ground movement normal to the pipeline axis. The testing setup, is depicted in Figure 26 whereas in Figure 27 the initial position of the pipe-specimen with respect to the soil boxes are presented schematically. This device consists of a 25-meter-long backfill, composed by three adjacent to each other soil boxes, in which the 8-inch-diameter 5.56-mm-thick X65 steel pipe specimen is buried. During testing, the central soil box can slide on rails and is pulled by two hydraulic actuators in a direction transverse to pipe axis, while the other two boxes remain fixed. Each actuator is capable of applying a maximum force equal to 400 tons, and has a stroke that exceeds 5 meters. As a result, the buried specimen is subjected to differential ground-induced action, associated with soil-pipe interaction forces, which cause pipe deflection and plastic bending deformations. As the pipe deforms transversally, its two ends are free to translate axially, while end rotations, as well as vertical and transverse displacements are prevented. A three-dimensional sketch of the test setup in given in Figure 26, in both initial and deformed configuration, whereas, pictures of the test arrangement are given in Figure 28 and Figure 29.

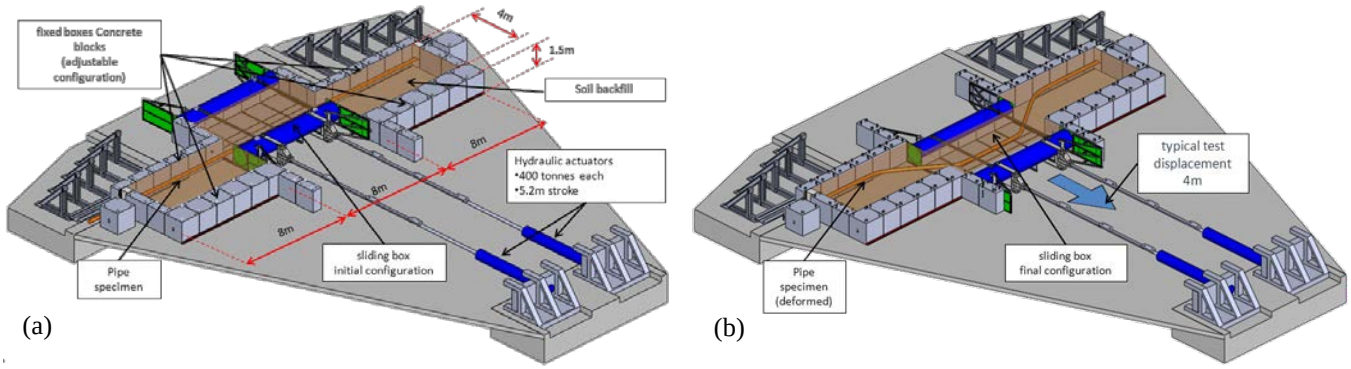

Figure 26. Three-dimensional representation of experimental setup for "landslide/fault" tests; (a) initial position; (b) deformed position.

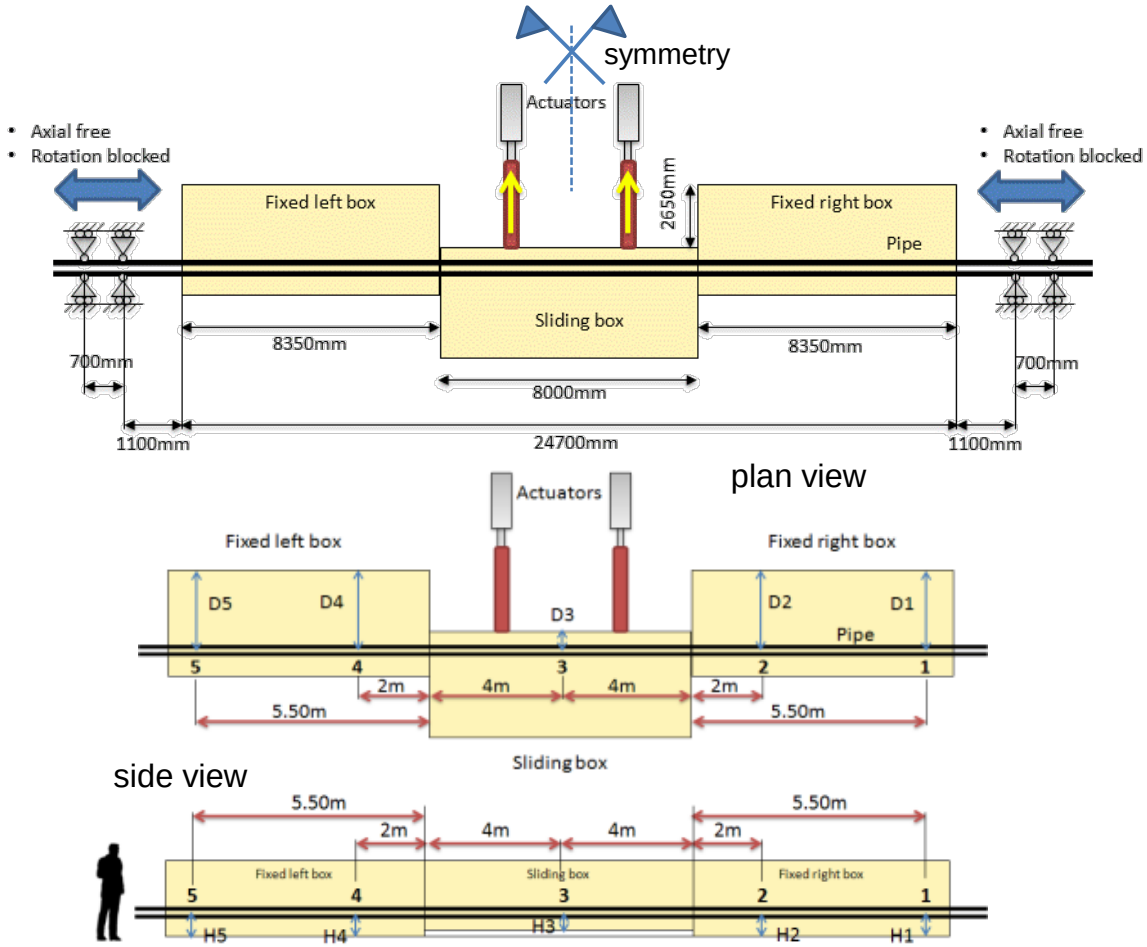

Figure 27. Vertical section and plan view of test setup (initial configuration); $H1 = H2 = H4 = H5 = 565$ mm, $H3 = 420$ mm, $D1 = D2 = D4 = D5 = 3720$ mm, $D3 = 750$ mm.

Figure 28. Soil boxes before sand filling and pipe specimen installation.

Figure 29. Views of experimental setup of "landslide/fault" tests; actuators and soil boxes.

5.2 Numerical simulation of full-scale tests

A finite element model has also been developed to simulate the "landslide/fault" testing procedure. The finite element model follows the general trends described in section 2, and is calibrated with the results presented in section 3 and 4. The model configuration is shown in Figure 30a; the middle box slides along the *x* axis, while the two outer boxes remain fixed at their base. The soil is simulated using reduce-integration solid elements (C3D8R) while the pipe was simulated using reduce-integration shell elements (type S4R). For test LD1, the modified Mohr-Coulomb model, described in previous sections, has been employed for the sand, while the developed subroutine FRIC described in sections 2 was used for the axial soil-pipe interaction. On the other hand for the tests LD2, LD3 and LD4 a classical Mohr-Coulomb model with internal angle of friction equal to φ_{res} and dilation angle equal to zero is employed for the sand while a bilinear friction law is assumed for axial soil-pipe interaction corresponding to φ_{res} and calculated according to methodology proposed in section 3. The finite element mesh of the model (Figure 30a) is considered fine enough especially in the cross section of the model with respect to pipe axis; this resulted in a substantial increase of the computational time. Figure 30b and Figure 30c present the deformed shape of pipe specimen and the distribution of the equivalent plastic shear strains from the numerical simulation of the first "landslide/fault" test (LD1).

Comparisons between the experimental results of test LD1 and the finite element predictions are shown in Figure 31 for middle box displacement equal to 200, 400 and 600 mm, corresponding to 0.91, 1.82 and 2.74 pipe diameters, respectively. The variation of longitudinal strain along a pipe generator in the front side (which refers to the side facing the two actuator) of the pipe is shown for half specimen length (due to symmetry, as shown in Figure 27); *x*=0 corresponds to symmetry plane. The comparison between numerical and experimental results is quite satisfactory, especially for displacement values equal to 400 and 600 mm, where significant plastic strains are developed in the pipe. On the other hand, for displacement of the central box equal to 200 mm, the pipe remains practically elastic. In this case the numerical model predicts the maximum compressive strain in a slightly different position, as shown in Figure 31(a). Similarly, in Figure 32, the longitudinal strains along the front-side generator are shown for tests LD2, LD3 and LD4. The comparison between the experimental measurements and the numerical results is also very satisfactory, indicating that this type of numerical model is capable of predicting accurately ground-induced strains on a buried pipe subjected to permanent ground deformation resulting from strike-slip fault or landslide actions.

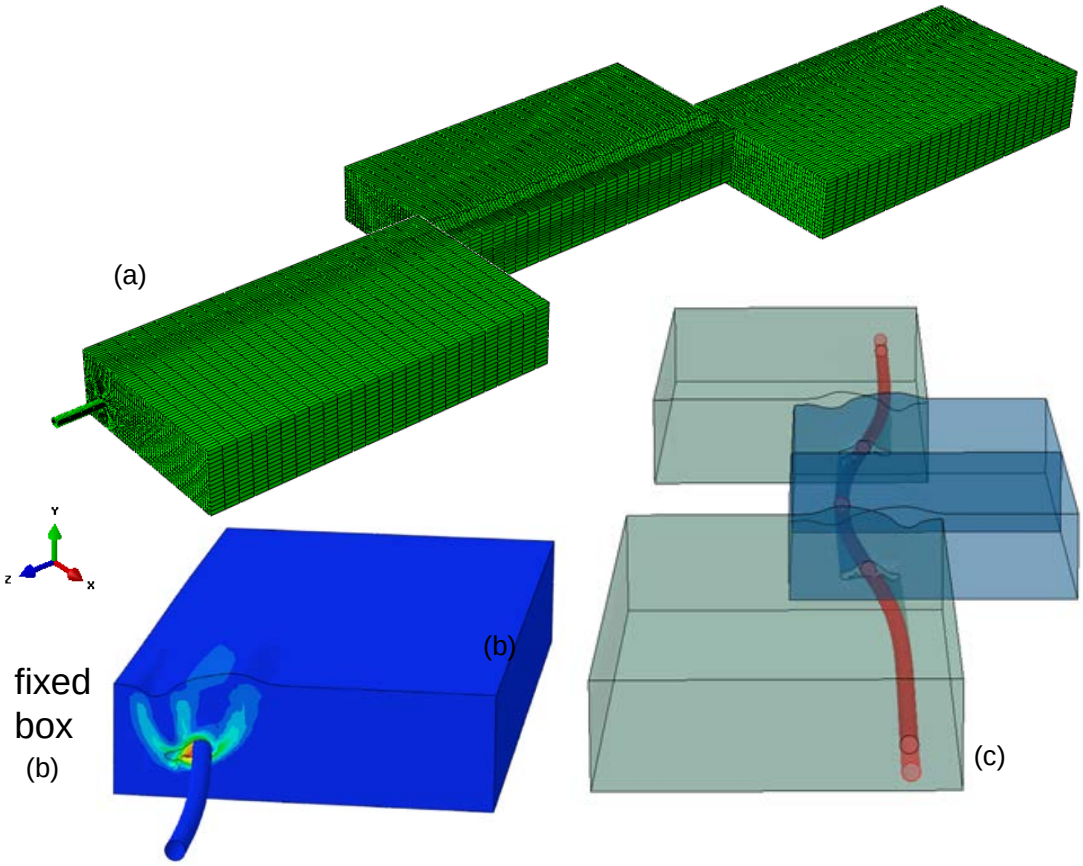

Figure 30. Numerical simulation of test LD1: (a) General configuration of the numerical model (b) Distribution of plastic strains in the middle block; (c) Deformed shape of the finite element model at imposed displacement equal to 600 mm (2.74 D).

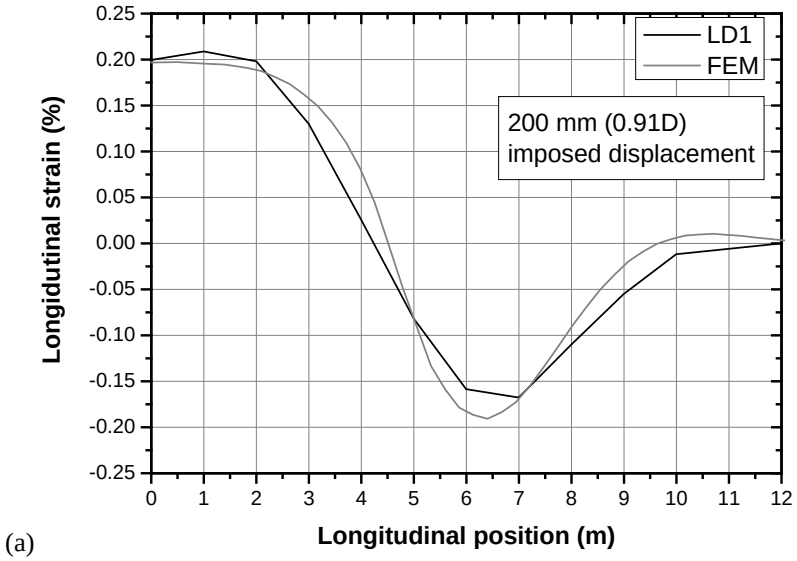

(a)

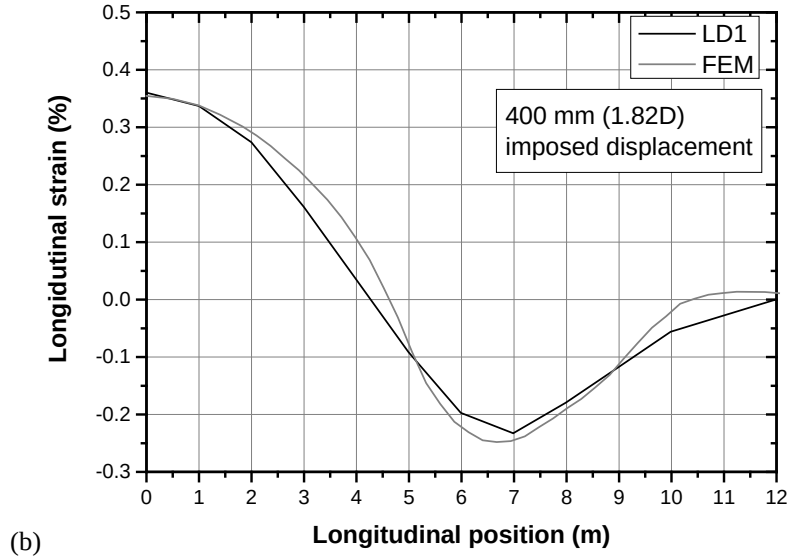

(b)

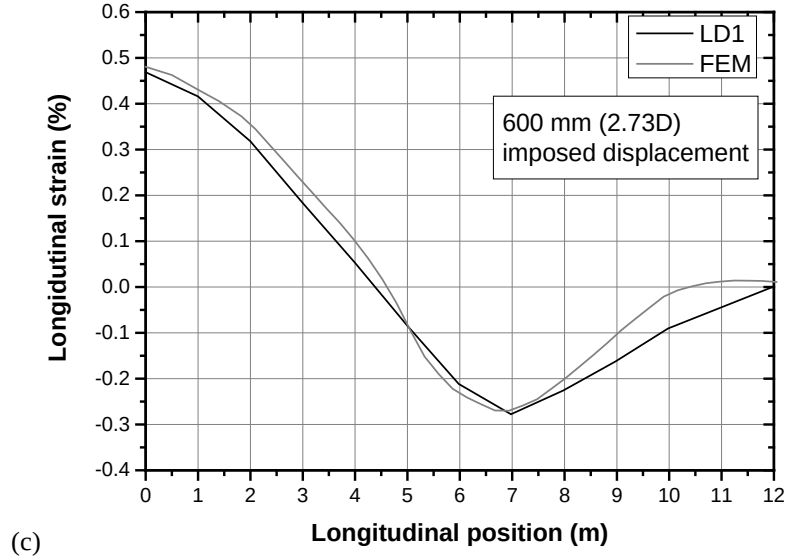

(c)

Figure 31. Comparison between experimental measurements and finite element predictions of test LD1 on longitudinal strains along the pipe; imposed displacement is equal to (a) 200 mm (0.91 D); (b) 400 mm (1.82 D); and (c) 600 mm (2.73 D).

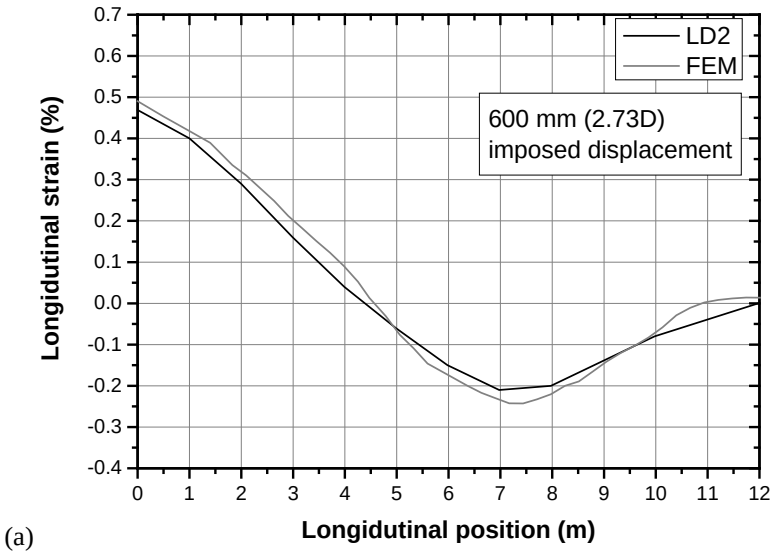

(a)

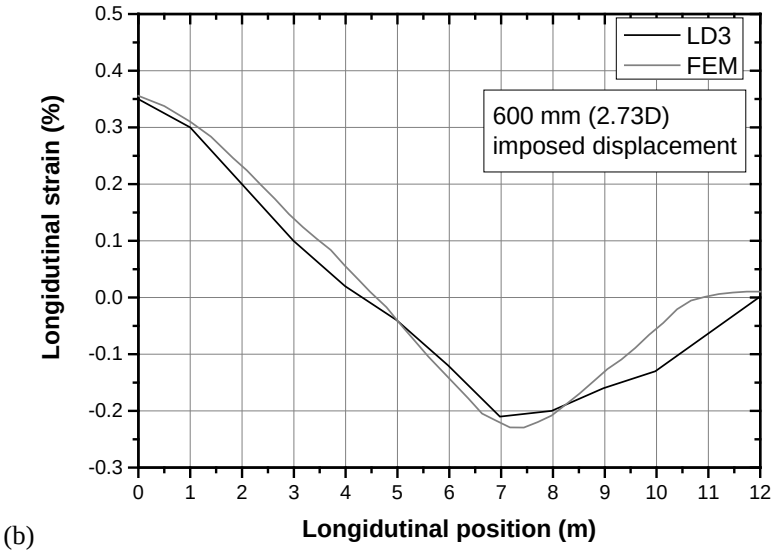

(b)

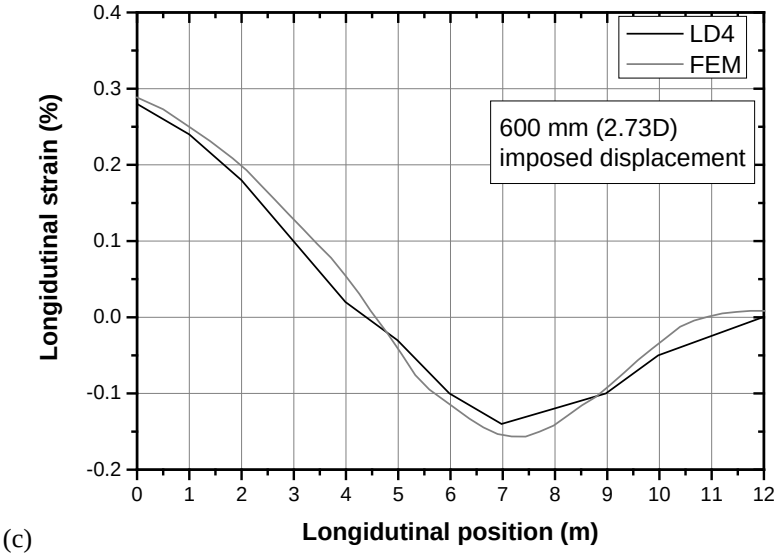

(c)

Figure 32. Comparison between experimental measurements and finite element predictions on longitudinal strains along the pipe; imposed displacement is equal to 600 mm (2.73 D): (a) test LD2; (b) test LD3; and (c) test LD4.

6 CONCLUSIONS

Soil-pipe interaction in buried pipelines, subjected to permanent earthquake-induced actions in sand (cohesionless) soil conditions, has been investigated using a combination of large-scale experimental testing and rigorous finite element simulations. The large-scale testing devices and equipment allowed for an accurate description of the physical phenomenon, reproducing the behavior of a real buried pipeline section undergoing earthquake-induced ground deformations in specific soil conditions, measuring soil-pipe interaction forces and pipe structural response. Furthermore, the numerical models are based on a rigorous three-dimensional finite element description of the coupled soil-pipe system, which employs solid elements and shell elements for the soil and the pipe respectively, and are validated using the experimental results.

Axial and horizontal-transverse soil-pipe interactions have been investigated extensively in the first part of the paper. The comparison between numerical and experimental results demonstrated that the rigorous numerical models, are capable of describing accurately the load-displacement response and the strains developed in buried pipelines under the permanent ground deformations.

The results demonstrate that, in the case of dense sand, soil dilatancy has a significant effect on axial soil-pipe interaction, and this effect should be taken into account in the numerical models for describing friction in the soil-pipe interface. Comparisons of experimental results with numerical predictions indicate that the actual behavior can be simulated quite accurately using a bilinear friction law, corresponding to the "peak" or the "residual" friction value of the soil. It should be noticed that in current design guidelines and recommendations, this dilatancy effect is not taken into account, and may result in overestimation of critical ground displacement in pipeline fault crossings.

In the transverse direction, soil-pipe interaction response is governed by the "residual" value of internal friction angle of sand. The results indicated that the use of classical Mohr-Coulomb constitutive model for the cohesionless soil is capable of simulating soil resistance in the transverse direction with good accuracy, using the residual value of internal angle of friction and assuming a zero value for the dilation angle. Experimental and numerical results are in good agreement with predictions from existing design guidelines and recommendations.

In the second part of the paper, the mechanical response of a buried steel pipeline subjected to complex loading conditions, is examined using a unique, special-purpose, large-scale "landslide/fault" testing device. Those large-scale tests have also been simulated with the rigorous three-dimensional finite element models and the comparison showed a good agreement between the experimental measurements and the relevant numerical predictions. This good comparison builds confidence on the numerical models, indicating that the proposed numerical models are capable of predicting quite satisfactory the mechanical response of buried steel pipelines subjected to permanent ground actions in earthquake and other geohazard areas and can be used in pipeline seismic design, whenever accuracy of numerical calculations is required.

7 ACKNOWLEDGEMENTS

This research work was carried out with a financial grant from the European Commission through the Research Fund for Coal and Steel Program, Contract No. RFSR-CT-2011-00027, **"**Safety of Buried Steel Pipelines Under Ground-Induced Deformations", project acronym GIPIPE [21]. The direct shear tests were performed by the Soil Mechanics Laboratory, National Technical University of Athens, Greece. The steel pipe specimens for the experimental testing have been provided by Corinth Pipe Works S.A., Thisvi, Greece.

8 REFERENCES

1. Newmark N. M. and Hall W. J. (1975), "Pipeline design to resist large fault displacement*". Proceedings of U.S. National Conference on Earthquake Engineering*, 416–425.
2. Kennedy, R. P., Chow, A. W. and Williamson, R. A. (1977), "Fault movement effects on buried oil pipeline", *ASCE Journal of Transportation Engineering*, **103**: 617-633.
3. Wang, L. R. L. and Yeh, Y. A. (1985), "A refined seismic analysis and design of buried pipeline for fault movement", *Earthquake Engineering & Structural Dynamics*, **13**: 75-96.
4. Takada, S., Hassani, N. and Fukuda, K. (2001), "A new proposal for simplified design of buried steel pipes crossing active faults", *Earthquake Engineering and Structural Dynamics*, **30**: 1243–1257.
5. Karamitros, D. K., Bouckovalas, G. D. and Kouretzis, G. P. (2007), "Stress Analysis of Buried Steel Pipelines at Strike Slip Fault Crossings", *Soil Dynamics & Earthquake Engineering*, **27:** 200-211.
6. Trifonov, O. V. and Cherniy, V. P. (2010), "A semi-analytical approach to a nonlinear stress–strain analysis of buried steel pipelines crossing active faults", *Soil Dynamics & Earthquake Engineerin*g, **30:** 1298-1308.
7. Trifonov, O. V. and Cherniy, V. P. (2012), "Elastoplastic stress strain analysis of buried steel pipelines subjected to fault

displacements with account for service loads", *Soil Dynamics & Earthquake Engineering*, **33**(1): 54-62.

8. Karamitros D. K., Bouckovalas G. D., Kouretzis G. P. and Gkesouli V. (2011), *"An Analytical Method for Strength Verification of Buried Steel Pipelines at Normal Fault Crossings"*, Soil Dynamics and Earthquake Engineering, **31**(11): 1452-1464.
9. ASCE (1984), *Guidelines for seismic design of oil and gas pipeline systems. Committee on Gas and Liquid Fuel Lifelines*, Technical Council on Lifeline Earthquake Engineering, American Society of Civil Engineers, Reston, Va.
10. American Lifelines Alliance, (2001), *Guidelines for the Design of Buried Steel Pipe*, New York, NY.
11. Vazouras, P., Karamanos, S. A. and Dakoulas, P. (2010), "Finite Element Analysis of Buried Steel Pipelines Under Strike-Slip Fault Displacements", *Soil Dynamics and Earthquake Engineering*, **30**(11): 1361–1376.
12. Trifonov, O. V. (2015), "Numerical Stress-Strain Analysis of Buried Steel Pipelines Crossing Active Strike-Slip Faults with an Emphasis on Fault Modelling Aspects", *ASCE Journal of Pipeline Systems Engineering and Practice*, **6**(1).
13. Kaya, E. S., Uckan, E., O'Rourke, M. J., Karamanos, S. A., Akbas, B., Cakir, F. and Cheng, Y. (2017), "Failure Analysis of a Welded Steel Pipe at Kullar Fault Crossing", *Engineering Failure Analysis*, **71**: 43-62.
14. Trautmann, C. H. and O'Rourke, T. D, (1985), "Lateral Force Displacement Response of Buried Pipe", *ASCE Journal of Geotechnical Engineering*, **111**(9): 1077-1092.
15. Ha, D., Abdoun, T., O'Rourke, M. J., Symans, M. D., O'Rourke, T. D., Palmer, M. C., and Stewart, H. E., (2008), "Centrifuge Modeling of Earthquake Faulting Effects on Buried HDPE Pipelines", *ASCE Journal of Geotechnical and Geoenvironmental Engineering*, **134**(10): 1501-1515.
16. Paulin, M. J., Phillips, R., Clark, J. I., Trigg, A. and Konuk, I. (1998), "A full-scale investigation into pipeline/soil interaction", *Proceedings of International Pipeline Conference*, ASME, Calgary, AB, Canada, 779-788.
17. Anderson, C. (2004), *Soil–pipeline interaction of polyethylene natural gas pipelines in sand*, M.Sc thesis, Department of Civil Engineering, University of British Columbia, Vancouver, B.C., Canada.
18. Scarpelli, G., Sakellariadi, E. and Furlani, G. (2003), "Evaluation of soil-pipeline longitudinal interaction forces", *Rivista Italiana di Geotecnica*.
19. Mortara, G., Boulon, M. and Ghionna, V. N. (2002), "A 2-D constitutive model for cyclic interface behaviour". *Int. J. Numerical Analytical Methods in Geomechanics*, **26**: 1071–1096. doi:10.1002/nag.236.
20. Karimian, H. (2006), *Response of buried steel pipelines subjected to longitudinal and transverse ground movement*. Ph.D. thesis, Department of Civil Engineering, The University of British Columbia, Vancouver, B.C.
21. Vazouras, P. *et al*. (2015), *Safety of Buried Steel Pipelines Under Ground-Induced Deformations*, Final Report, GIPIPE project, RFSR-CT-2011-00027, Research Fund for Steel and Coal (RFCS), Brussels, Belgium, available at https://publications.europa.eu/en/web/general-publications/publications.
22. Vazouras, P., Karamanos, S. A., and Dakoulas, P. (2012), "Mechanical behavior of buried steel pipes crossing active strike-slip faults", *Soil Dynamics and Earthquake Engineering*, **41**: 164–180.
23. Vazouras, P., Dakoulas, P., and Karamanos, S. A. (2015), "Pipe-Soil Interaction and Pipeline Performance Under Strike-Slip Fault Movements", *Soil Dynamics and Earthquake Engineering*, **72**: 48-65.
24. Tsatsis, A., Anastasopoulos, I. and Gazetas, G. (2015), "Buried pipelines subjected to normal fault: Simulation vs experiment", *Geotechnical Engineering for Infrastructure and Development - Proceedings of the XVI European Conference on Soil Mechanics and Geotechnical Engineering*, ECSMGE 2015, **6**: 3407-3412.
25. Sarvanis, G. C. and Karamanos, S. A. (2017), "Analytical model for the strain analysis of continuous buried pipelines in geohazard areas", *Engineering Structures*, **152**: 57-69.
26. Van Es, S. H. J. and Gresnigt A. M. (2016), "Experimental and Numerical Investigation into the Behavior of Buried Steel Pipelines Under Strike-Slip Fault Movement", *ASME International Pipeline Conference*, **1***: Pipelines and Facilities Integrity*, IPC2016-64095, Calgary, Alberta, Canada.
27. Sarvanis, G. C., Ferino, J., Karamanos, S. A., Vazouras, P., Dakoulas, P., Mecozzi, E. and Demofonti, G. (2016), "Soil-Pipe Interaction Models for Simulating the Mechanical Response of Buried Steel Pipelines Crossing Active Faults.", *International Society of Offshore and Polar Engineers*, ISOPE 2016, Rhodes, Greece.
28. Anastasopoulos I., Gazetas G., Bransby M. F., Davies M. C. R. and El Nahas A. (2007), "Fault rupture propagation through sand: finite element analysis and validation through centrifuge experiments", *ASCE Journal of Geotechnical and Geoenvironmental Engineering*, **133**(8): 943–958.
29. ABAQUS Users' Manual (2013), Simulia, Pawtucket, Rhode Island.